


RESEARCH

Open Access



Nano-titanium dioxide inhalation exposure during gestation drives redox dysregulation and vascular dysfunction across generations

Elizabeth C. Bowdridge^{1,2†}, Evan DeVallance^{1,2†}, Krista L. Garner^{1,2}, Julie A. Griffith^{1,2}, Kallie Schafner^{1,2}, Madison Seaman¹, Kevin J. Engels¹, Kimberley Wix¹, Thomas P. Batchelor^{1,2}, William T. Goldsmith^{1,2}, Salik Hussain^{1,2} and Timothy R. Nurkiewicz^{1,2*} 

Abstract

Background: Pregnancy is associated with many rapid biological adaptations that support healthy development of the growing fetus. One of which is critical to fetal health and development is the coordination between maternal liver derived substrates and vascular delivery. This crucial adaptation can be potentially derailed by inhalation of toxicants. Engineered nanomaterials (ENM) are commonly used in household and industrial products as well as in medicinal applications. As such, the potential risk of exposure remains a concern, especially during pregnancy. We have previously reported that ENM inhalation leads to upregulation in the production of oxidative species. Therefore, we aimed to determine if F0 dam maternal nano-TiO₂ inhalation exposure (exclusively) resulted in altered H₂O₂ production capacity and changes in downstream redox pathways in the F0 dams and subsequent F1 pups. Additionally, we investigated whether this persisted into adulthood within the F1 generation and how this impacted F1 gestational outcomes and F2 fetal health and development. We hypothesized that maternal nano-TiO₂ inhalation exposure during gestation in the F0 dams would result in upregulated H₂O₂ production in the F0 dams as well as her F1 offspring. Additionally, this toxicological insult would result in gestational vascular dysfunction in the F1 dams yielding smaller F2 generation pups.

Results: Our results indicate upregulation of hepatic H₂O₂ production capacity in F0 dams, F1 offspring at 8 weeks and F1 females at gestational day 20. H₂O₂ production capacity was accompanied by a twofold increase in phosphorylation of the redox sensitive transcription factor NF-κB. In cell culture, naïve hepatocytes exposed to F1-nano-TiO₂ plasma increased H₂O₂ production. Overnight exposure of these hepatocytes to F1 plasma increased H₂O₂ production capacity in a partially NF-κB dependent manner. Pregnant F1-nano-TiO₂ females exhibited estrogen disruption (12.12 ± 3.1 pg/ml vs. 29.81 ± 8.8 pg/ml sham-control) and vascular dysfunction similar to their directly exposed mothers. F1-nano-TiO₂ uterine artery H₂O₂ production capacity was also elevated twofold. Dysfunctional gestational outcomes in the F1-nano-TiO₂ dams resulted in smaller F1 (10.22 ± 0.6 pups vs. sham-controls 12.71 ± 0.96 pups) and F2 pups (4.93 ± 0.47 g vs. 5.78 ± 0.09 g sham-control pups), and fewer F1 male pups (4.38 ± 0.3 pups vs. 6.83 ± 0.84 sham-control pups).

*Correspondence: tnurkiewicz@hsc.wvu.edu

[†]Elizabeth C. Bowdridge and Evan DeVallance are co-first authors

¹ Department of Physiology and Pharmacology, 64 Medical Center Drive, Robert C. Byrd Health Sciences Center, West Virginia University School of Medicine, West Virginia University, Morgantown, WV 26505-9229, USA
Full list of author information is available at the end of the article



© The Author(s) 2022. **Open Access** This article is licensed under a Creative Commons Attribution 4.0 International License, which permits use, sharing, adaptation, distribution and reproduction in any medium or format, as long as you give appropriate credit to the original author(s) and the source, provide a link to the Creative Commons licence, and indicate if changes were made. The images or other third party material in this article are included in the article's Creative Commons licence, unless indicated otherwise in a credit line to the material. If material is not included in the article's Creative Commons licence and your intended use is not permitted by statutory regulation or exceeds the permitted use, you will need to obtain permission directly from the copyright holder. To view a copy of this licence, visit <http://creativecommons.org/licenses/by/4.0/>. The Creative Commons Public Domain Dedication waiver (<http://creativecommons.org/publicdomain/zero/1.0/>) applies to the data made available in this article, unless otherwise stated in a credit line to the data.

Conclusion: In conclusion, this manuscript provides critical evidence of redox dysregulation across generations following maternal ENM inhalation. Furthermore, dysfunctional gestational outcomes are observed in the F1-nano-TiO₂ generation and impact the development of F2 offspring. In total, this data provides strong initial evidence that maternal ENM exposure has robust biological impacts that persists in at least two generations.

Keywords: Engineered nanomaterials, Titanium dioxide, Microcirculation, Kisspeptin, Placenta

Introduction

A myriad of anatomical and physiological adaptations must take place throughout gestation for a successful pregnancy to occur. Hepatic and vascular adaptation and growth coordinate substrate availability and delivery to the developing fetus [1–3]. This complex, highly regulated, maternal circuit is sensitive to potential toxicant disruption. In 2013, the National Institute of Environmental Health Sciences (NIEHS), formally acknowledged the rise in incidences of adverse pregnancy outcomes associated with exposure to endocrine disrupting chemicals [4]. Even though only the mother is being directly exposed, her offspring and their reproductive capacity may be affected by this gestational insult. The basis for such adult disease can originate from inadequacies of blood flow/substrate delivery during development, which may create a hostile gestational environment and ultimately lead to utero-placental insufficiency. Originally developed by Barker, this theory is recognized as the developmental origins of health and disease (DOHaD) [5, 6]. Inhalation exposure during gestation has the potential to lead to multi- and transgenerational effects. During a toxicological insult, the mother is directly exposed, but the F1 generation experiences a hostile gestational environment during fetal development, and the F2 generation is also subject to this insult as the developing germ cell line with the F1 offspring. If negative health consequences persist into the F3 generation, without subsequent exposure, this is considered a transgenerational effect because these offspring have never been exposed to particles or a hostile gestational environment associated with the original F0 insult [7]. Nano-TiO₂ has been shown to cross the placenta [8] during gestational exposure and potentially deposits into the pup [9], however perturbations in vasoreactivity within the uterus of the dam and/or the placenta of the pup alone are enough to result in detrimental fetal health consequences [10].

Engineered nanomaterials (ENM) are defined as materials with at least one dimension less than 100 nm and unique physiochemical properties [11]. The potential toxicity of ENM in biological systems remains an area of specific interest to the National Toxicology Program [12]. Many variables influence the toxicokinetics of a given chemical all of which ultimately focus on dose. We have previously established that a calculated lung deposition

of ~ 30 µg per exposure is associated with a ~ 50% impairment in normal arteriolar function [13]. While many factors such as absorption, distribution, and clearance influence toxicity we focused on dose, specifically deposition in this study. Our previous work demonstrated that inhalation exposure to an ENM, such as nano-titanium dioxide (nano-TiO₂), during gestation disrupts normal uterine [14] and pup [15] arteriolar function [14], placental hemodynamics [16] fetal pup weight, and placental efficiency [10]. However, scant evidence exists as to the underlying mechanisms of these findings and the systemic impact on the subsequent offspring.

Recently, we reported that maternal nano-TiO₂ inhalation during gestation can result in endocrine disruption, specifically estrogen [10]. During gestation, the peptide hormone kisspeptin (Kiss) [17–19], is associated with hypertension, preeclampsia, and intrauterine growth restriction (IUGR) [20]. We found an augmented Kiss-induced vasoconstriction in uterine arteries of nano-TiO₂ exposed dams [10]. Interestingly, circulating Kiss levels were not different despite significantly decreased estrogen levels in this study [10]. Hypothalamically, low levels of estrogen are inhibitory to Kiss production whereas higher estrogen levels stimulate Kiss [21]. It is possible that circulating or local levels of estrogen are permissive to Kiss vasoreactivity in the uterine vasculature. This strongly suggests alterations in converging or competing cellular pathways account for the differential Kiss responses following nano-TiO₂ inhalation exposure.

Redox signaling pathways are critical in maintaining cellular homeostasis and dysregulation of these pathways contribute to several pathologies [22–25]. Hydrogen peroxide is one of the major reactive signaling molecules. Upregulation of H₂O₂-mediated production is linked to NF-κB-mediated signaling [26, 27], which is known to mediate both vascular and hepatic dysfunction [28, 29]. It has been reported that pulmonary exposure and estrogen deficiency lead to localized and systemic changes in cellular redox signaling [30–34], but the consequences of these perturbations during gestation on maternal and fetal health are vastly understudied. Redox signaling mediated by H₂O₂-regulation of signaling factors can influence multiple hepatic and vascular processes [35]. Interestingly, Kiss has been shown to contribute to the antioxidant defense system within the porcine follicle

[22–29, 36]. Whether maternal nano-TiO₂ inhalation disrupts H₂O₂-mediated signaling in critical tissues during pregnancy or whether redox signaling is altered in the F1 generation is unexplored.

Our previous work demonstrates maternal ENM inhalation exposure during gestation perturbs uterine vascular function [10]. Thus setting our rationale for investigating nano-TiO₂-mediated impacts on the subsequent offspring, based on the DOHaD theory. Therefore, the purpose of this study was to investigate redox signaling in both mother and offspring and determine if the previously defined Kiss response was present during pregnancy in the F1 generation. We hypothesized

that inhalation exposure during gestation in the F0 dams leads to vascular, and redox dysfunction that propagates to the F1 generation, and results in smaller F2 pups.

Results

Experiment 1

Characterization of nano-TiO₂

The nano-TiO₂ aerosol concentration was determined to be 12.35 ± 0.13 mg/m³ (Fig. 1A). The ELPI High Resolution data indicated a Geometric Count Median Diameter of 170 nm with a Geometric Standard Deviation of 1.95 (Fig. 1B). The SMPS and APS data were combined to determine the Geometric Count Median Diameter using

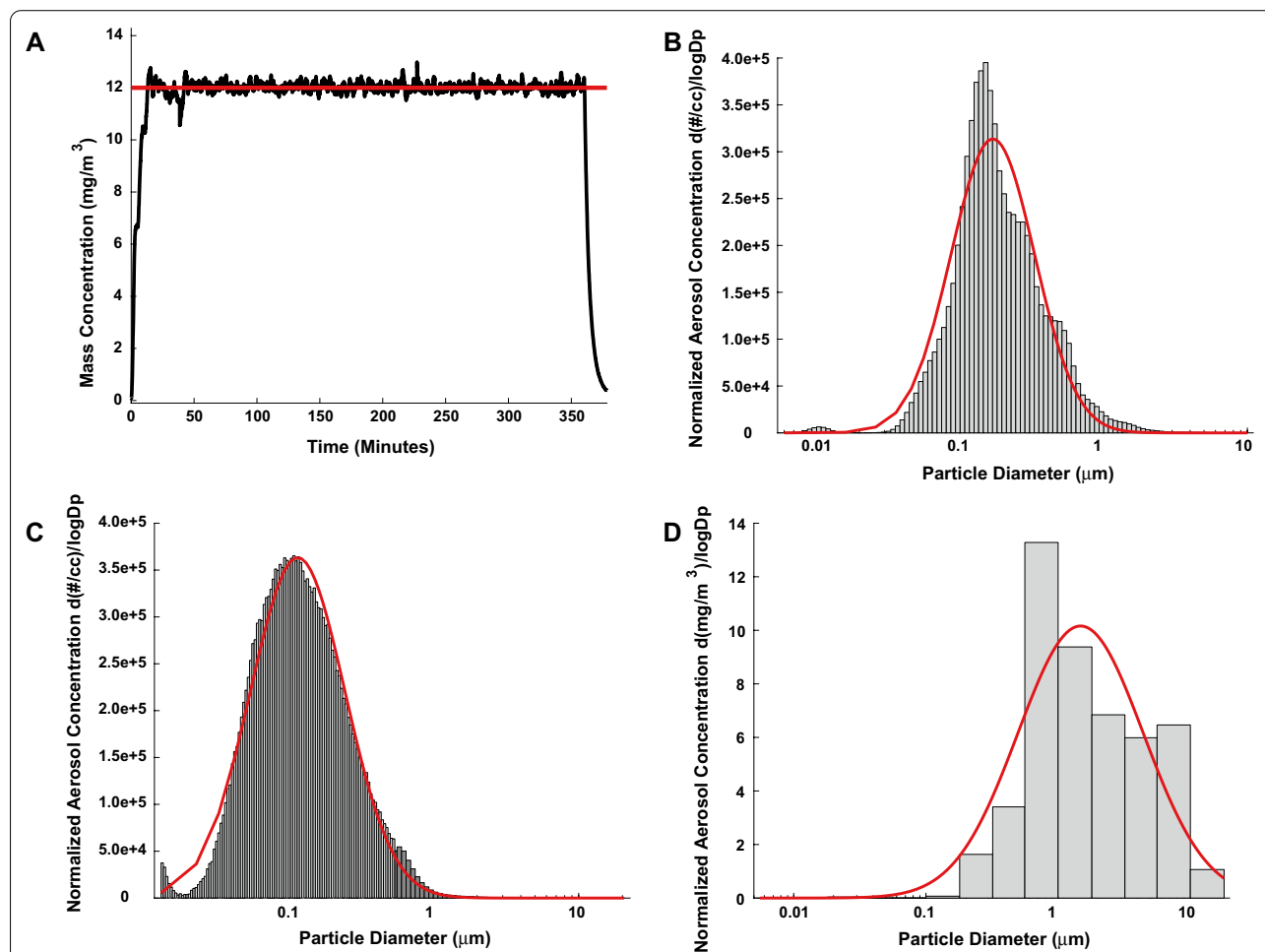


Fig. 1 Characterization of nano-TiO₂. **A** Representative real-time mass concentration measurements of the nano-TiO₂ aerosol during a typical inhalation exposure. The red line represents the target concentration, 12.35 ± 0.13 mg/m³. **B** Size distribution of the nano-TiO₂ aerosol (aerodynamic diameter) using a high-resolution electrical low-pressure impactor (ELPI+). The red line represents a log-normal fit of the histogram (count median diameter = 170) and geometric standard deviation (GSD) or 1.95. **C** Size distribution of the nano-TiO₂ aerosol (mobility diameter) sampled from the exposure chamber using a scanning mobility particle sizer (SMPS—light gray) and an aerodynamic particle sizer (APS—dark gray, negligible values). The red line is representative of a log-normal fit of the histogram (count median diameter = 116 nm) with a GSD or 2.12. **D** Mass size distribution of TiO₂ aerosols sampled from the exposure chamber with a Nano Micro-Orifice Uniform Deposit Impactor (MOUDI 115R, MSP Corp, Shoreview, MN). The red line represents a log normal fit of the data that indicates a mass median aerodynamic diameter (MMAD) of 1.48 μm with a GSD of 2.98

the log normal distribution obtained with the log probability plot method and was determined to be 116 nm with a Geometric Standard Deviation of 2.12 (Fig. 1C). Figure 1D is the mass size distribution of nano-TiO₂ aerosols sampled from the exposure chamber with a Nano Micro-Orifice Uniform Deposit Impactor (MOUDI 115R, MSP Corp, Shoreview, MN). The mass median aerodynamic diameter of 1.48 μm with a geometric standard deviation of 2.98.

Hepatic and placental redox activity of F0 dams and F1 progeny, and F1 litter characteristics

F0 maternal liver characteristics It is well documented that liver mass increases in proportion to body weight gain during pregnancy. Comparing maternal liver mass at GD 20, nano-TiO₂ exposed mothers' livers were significantly greater than those of sham-control mothers, even after normalization to body weight (Fig. 2A, B). Additionally, ALT but not AST was elevated at GD 20, nano-TiO₂ exposed mothers (Fig. 2C, D). We then analyzed H₂O₂ production capacity in maternal livers and found nano-TiO₂ exposed maternal livers exhibit roughly sixfold higher H₂O₂ production capacity (Fig. 2E). Concomitantly, lower levels of reduced GSH and a diminished

GSH:GSSH ratio were found (Fig. 2F–H). Supporting this elevated H₂O₂ signaling we found elevated activation of ERK and p-p65 as a marker of NF-κB (Fig. 2I–J). Together, this suggests redox homeostasis/signaling is altered in the maternal liver following nano-TiO₂ inhalation exposure. This is an impactful observation due to the critical role the maternal liver plays in fetal substrate regulation.

F1 litter characteristics F1 litter size was significantly reduced when F0 dams were exposed to nano-TiO₂ (10.22 ± 0.6 pups) during gestation compared to sham-controls (12.71 ± 0.96 pups; Table 1). Additionally, fewer male pups were born in nano-TiO₂ litters (4.38 ± 0.3 pups vs. 6.83 ± 0.84 pups exposed vs. sham-control, respectively). Nano-TiO₂ dams also displayed an increased number of pup resorptions, which was indicated by significantly more implantation sites compared to pups born alive (13.6 ± 1.27 spots vs. 10.22 ± 0.6 pups) compared to sham-controls (12.25 ± 0.79 spots vs. 12.71 ± 0.96 pups; *p* < 0.05; Table 1). Placental tissue displayed greater H₂O₂ production capacity in the nano-TiO₂ exposed group compared to sham-control (Fig. 3A). Similar to maternal livers, fetal livers of mothers exposed to nano-TiO₂ exhibit greater H₂O₂

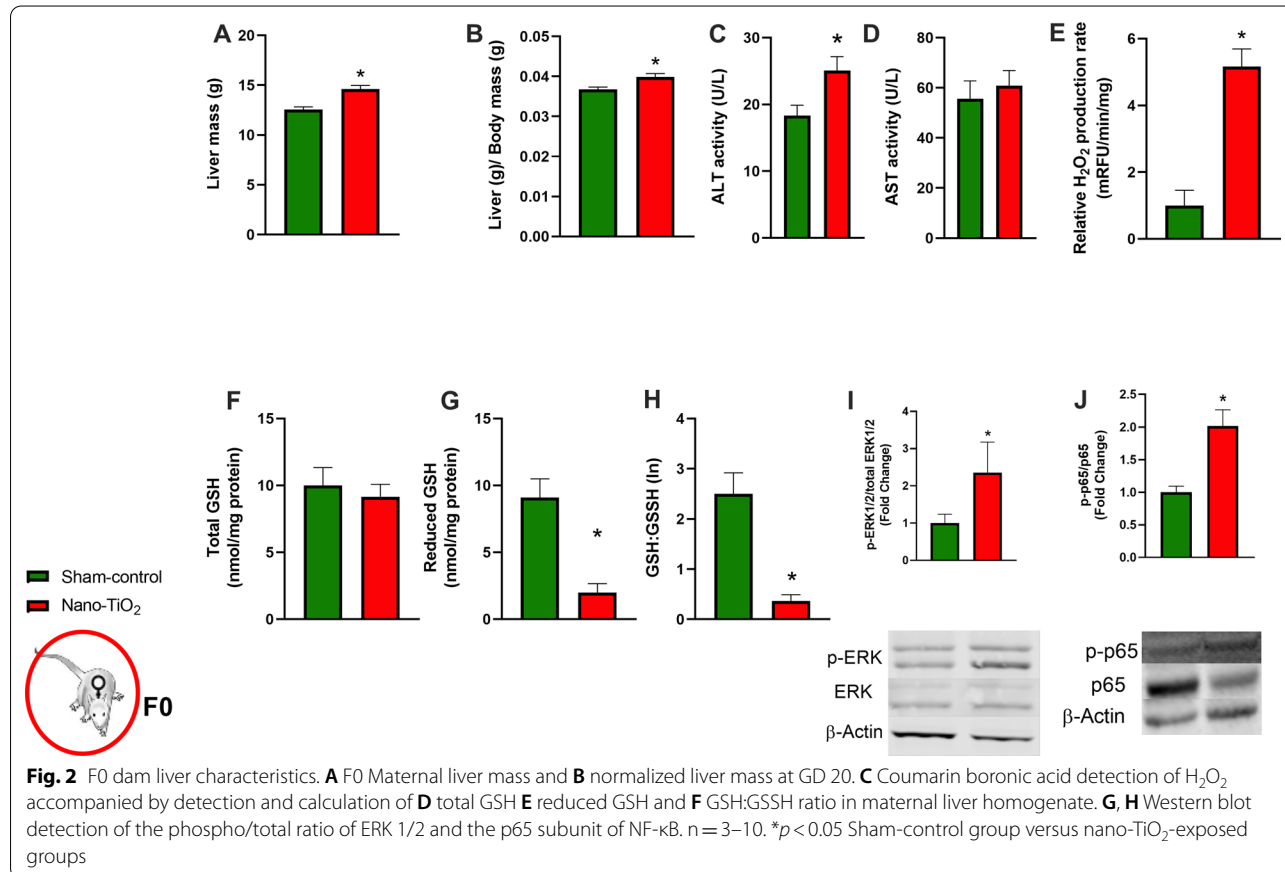
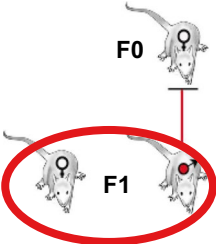
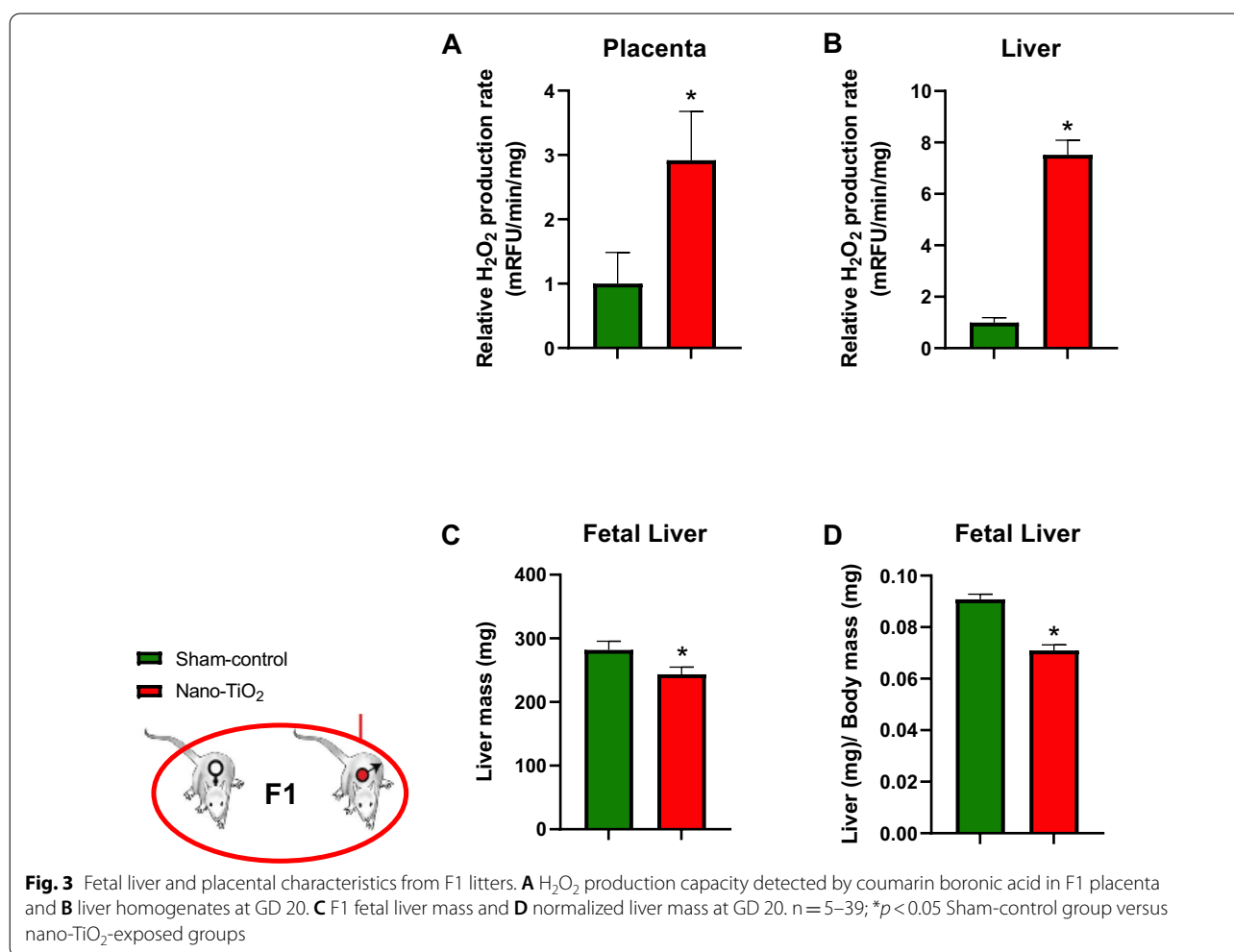


Table 1 Litter characteristics from F0 dams


	N	Litter size	Male pups	Female pups	Uterine weight	Implantation spots
Sham-control	7	12.71 ± 0.96	6.83 ± 0.84	6.83 ± 0.84	0.70 ± 0.06	12.25 ± 0.79
Nano-TiO₂ exposed	9	10.22 ± 0.6*	4.38 ± 0.3*	6.25 ± 0.88	0.71 ± 0.07	13.6 ± 1.27**

Dam and litter characteristics in sham-control (N = 7) and nano-TiO₂ inhalation exposed (N = 9) groups. Values are shown as mean ± SEM.

p* < 0.05 Sham-control group versus nano-TiO₂-exposed groups. *p* < 0.05 Litter size versus implantation spots in nano-TiO₂-exposed group.



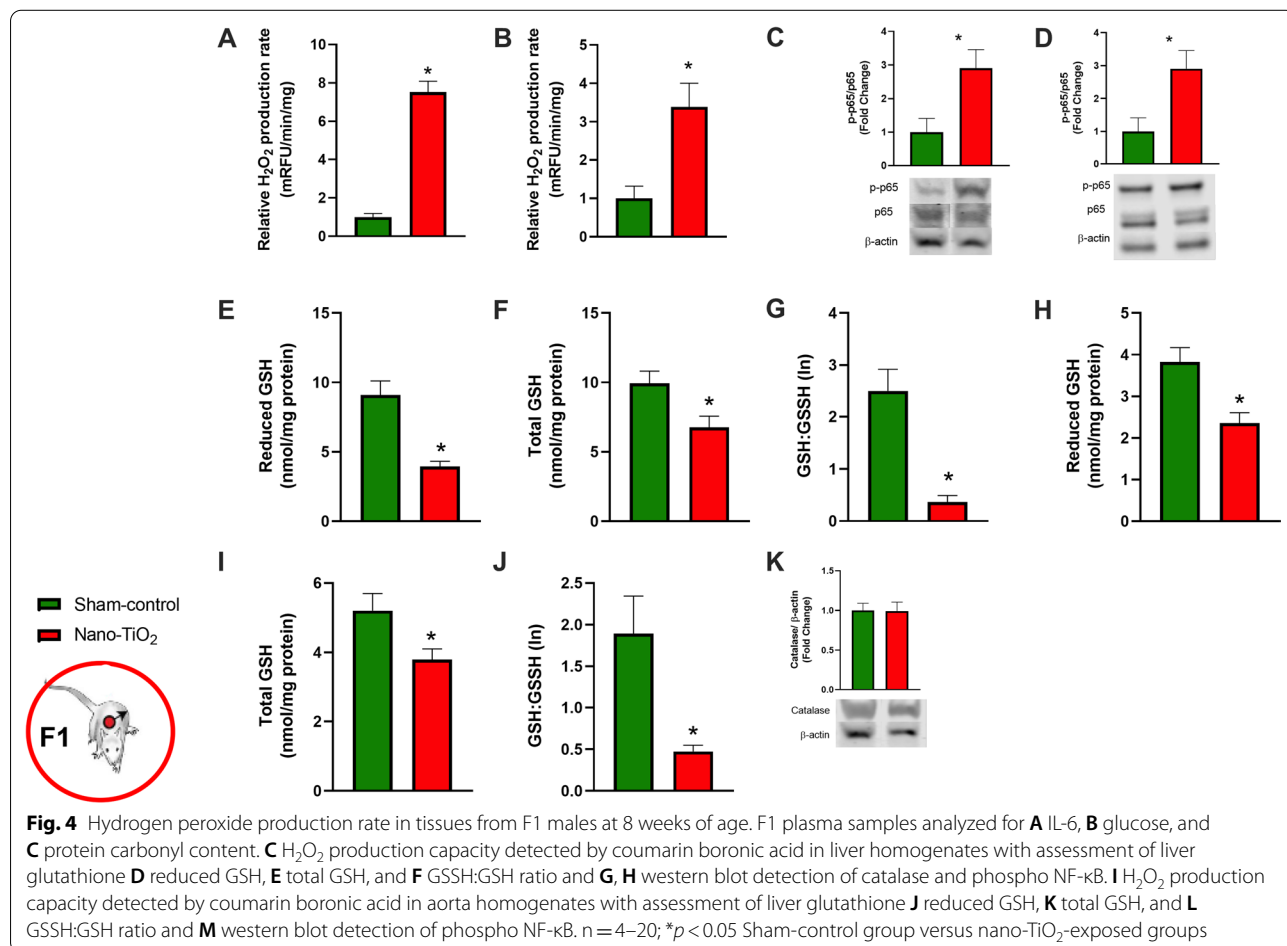
production capacity (Fig. 3B). We previously reported at GD 20 pups of mothers exposed to nano-TiO₂ were significantly smaller [10]. Consistent with this previous observation nano-TiO₂ pups also exhibited less liver mass (Fig. 3C). However, livers from nano-TiO₂ pups were significantly small even after normalization

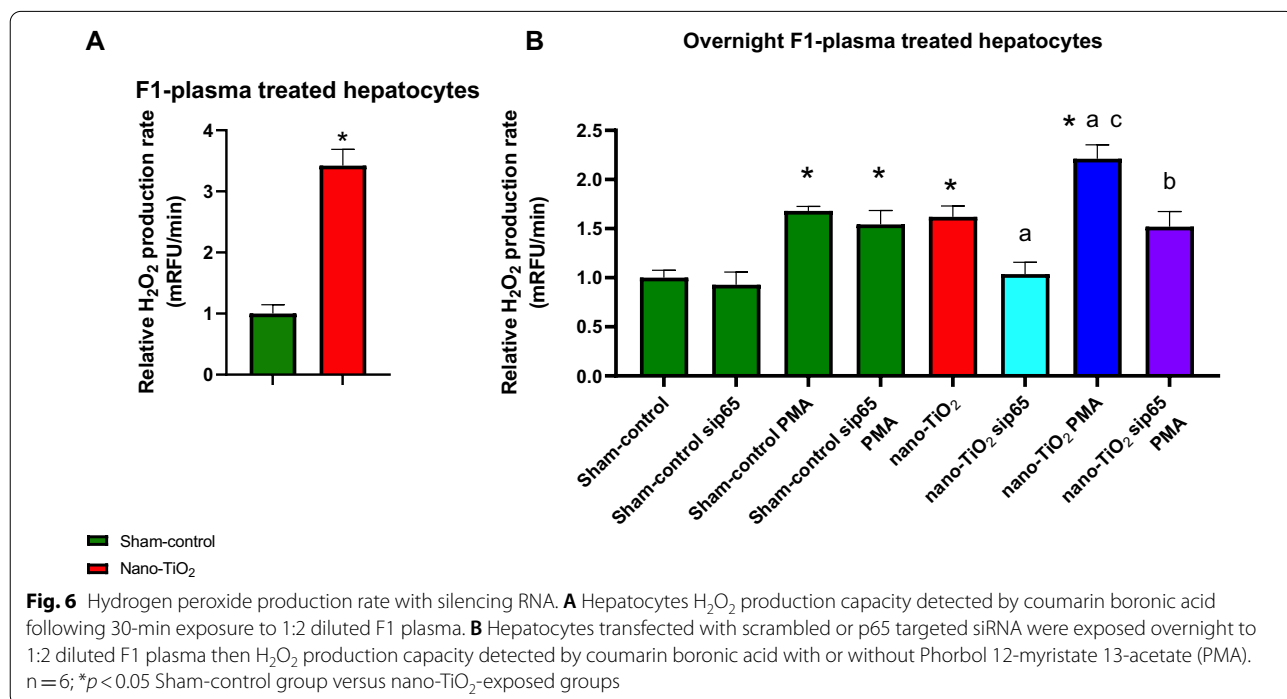
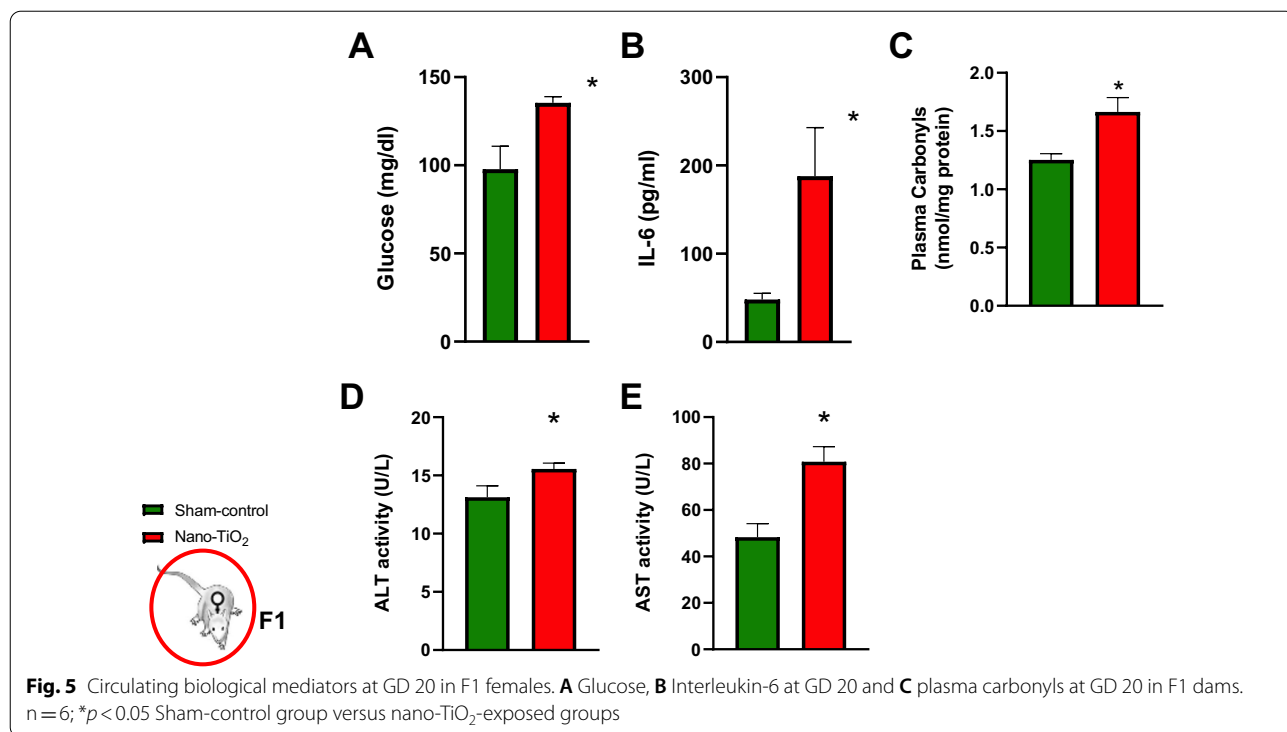
to body weight on GD 20 (Fig. 3D). Therefore, we can conclude that nano-TiO₂ inhalation exposure during gestation results in decreased litter size, potentially through causing resorption of fetuses, and skews the sex ratio of the offspring such that males seem to be more greatly affected by maternal ENM exposure. Considered

together, nano-TiO₂ inhalation exposure alters hepatic mass and induces redox dysfunction in dams as well as their progeny.

F1 systemic redox dysfunction Male offspring, 8 weeks of age, born to mothers exposed to nano-TiO₂ have higher capacity to produce H₂O₂ in liver, aorta (Fig. 4A, B), brain, pancreas, and lung compared to sham-controls (Additional file 1: Figure S1A–C). Western blot analysis showed elevated p-p65 levels in both the aorta and the liver of nano-TiO₂ offspring (Fig. 4C, D). Additionally, the glutathione antioxidant system is diminished in aorta and liver, presenting with lower total, reduced GSH, and GSH:GSSH ratio (Fig. 4E–J). However, the robust catalase levels in the liver appear unaltered (Fig. 4K). Additionally, in the plasma of F1 dams at GD 20 we detected elevated levels of glucose, IL-6, protein carbonyls, ALT and AST (Fig. 5). Finding elevations of known H₂O₂ inducers in the plasma we conducted experiments to determine if plasma factors (collected from F1 offspring at 8 weeks

of age; n = 8) could drive H₂O₂ production capacity in hepatocytes. First, acute exposure of a hepatic cell line to 1:2 diluted plasma from nano-TiO₂ F1 induced a threefold increase in H₂O₂ production capacity compared to sham-control plasma (Fig. 6A). To assess the impact of these plasma factors on “long term” hepatic redox regulation, cells were incubated with 1:2 diluted plasma overnight with or without siRNA against p65 subunit of NF-κB. Hepatic cells exposed to F1 nano-TiO₂ plasma exhibited greater H₂O₂ production capacity without stimulation. Furthermore, these cells exposed to F1 nano-TiO₂ plasma had a higher capacity to produce H₂O₂ when stimulated with 5 μM PMA. This capacity was abrogated in large part in hepatic cells transfected with 10 nM siRNA against p65 (Fig. 6B). It is clear from this data that redox dysfunction persists into adulthood in pups born to nano-TiO₂ exposed dams. This clearly demonstrates that circulating factors found within the plasma of adults born to nano-TiO₂ expose dams induces short- and long-term hepatic redox dysfunction.





Experiment 2

Pup weight, placenta weights and placental efficiency in F2 litters

Litter size (11.53 ± 0.68 pups vs. 9.52 ± 0.57 pups), wet (5.78 ± 0.09 g vs. 4.93 ± 0.47 g) and dry pup weight (Additional file 2: Table S1), and wet placental efficiency (7.51 ± 0.29 vs. 6.48 ± 0.18) were all significantly reduced in F2 litters born to F1 dams with nano-TiO₂ mothers when compared to F1 dams with sham-control mothers (Table 2). This is of note because despite not being exposed during gestation, dams born to nano-TiO₂ exposed dams still demonstrated poor gestational and fetal health outcomes at GD 20.

Uterine artery characteristics

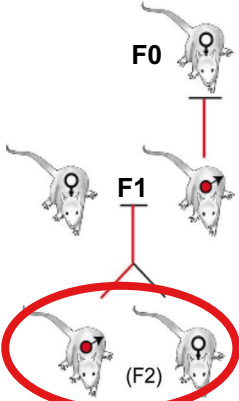
Turning our attention to female F1 nano-TiO₂ offspring, we were interested in looking again at the uterine vasculature at GD 20. Sham-control and nano-TiO₂-exposed uterine arteries had similar outer diameters (sham-control = 705 ± 51 μ m vs. exposed

643 ± 33 μ m). However, the inner diameter was significantly smaller in nano-TiO₂ exposed uterine arteries (502 ± 29 μ m) compared to sham-control (591 ± 35 μ m) and had increased tone ($38 \pm 4\%$ vs. $25 \pm 2\%$ exposed and sham-control vessels, respectively). (Table 3). These observations point to local vascular dysfunction during gestation that persists in F1 pups born to nano-TiO₂ exposed mothers.

Vasoreactivity assessments

Similar to our observations in uterine arteries from F0 dams that were directly exposed to nano-TiO₂ during gestation [9], uterine arteries from F1 dams born to mothers exposed to nano-TiO₂ demonstrated an augmented vasoconstrictor response to Kiss (15.83% overall diameter decrease in nano-TiO₂ exposed vs. 1.2% in sham-control $p < 0.05$; Fig. 7D). Additionally, F1 uterine arteries from dams born to exposed mothers had an augmented response to PE at the 10^{-4} M dose (Fig. 7C). No other point-to-point differences were seen between groups when vessels were treated with endothelium-dependent

Table 2 Pup and placental characteristics from F1 dams at GD 20

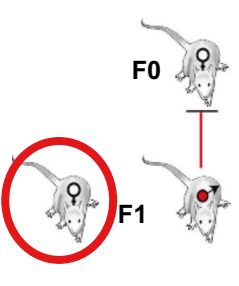


	N	Litter size	Pup wet weight (grams)	Placental wet weight (grams)	Placental efficiency (grams fetus/ grams placenta)
Sham-control	9	11.53 ± 0.68	5.78 ± 0.09	0.82 ± 0.03	7.51 ± 0.29
Nano-TiO₂ exposed	10	$9.52 \pm 0.57^*$	$4.93 \pm 0.47^*$	0.80 ± 0.02	$6.48 \pm 0.18^*$

Pup and placental characteristics in sham-control (N=9) and nano-TiO₂ inhalation exposed (N=10) groups. Values are shown as mean \pm SEM.

* $p < 0.05$ Sham-control group versus nano-TiO₂-exposed groups.

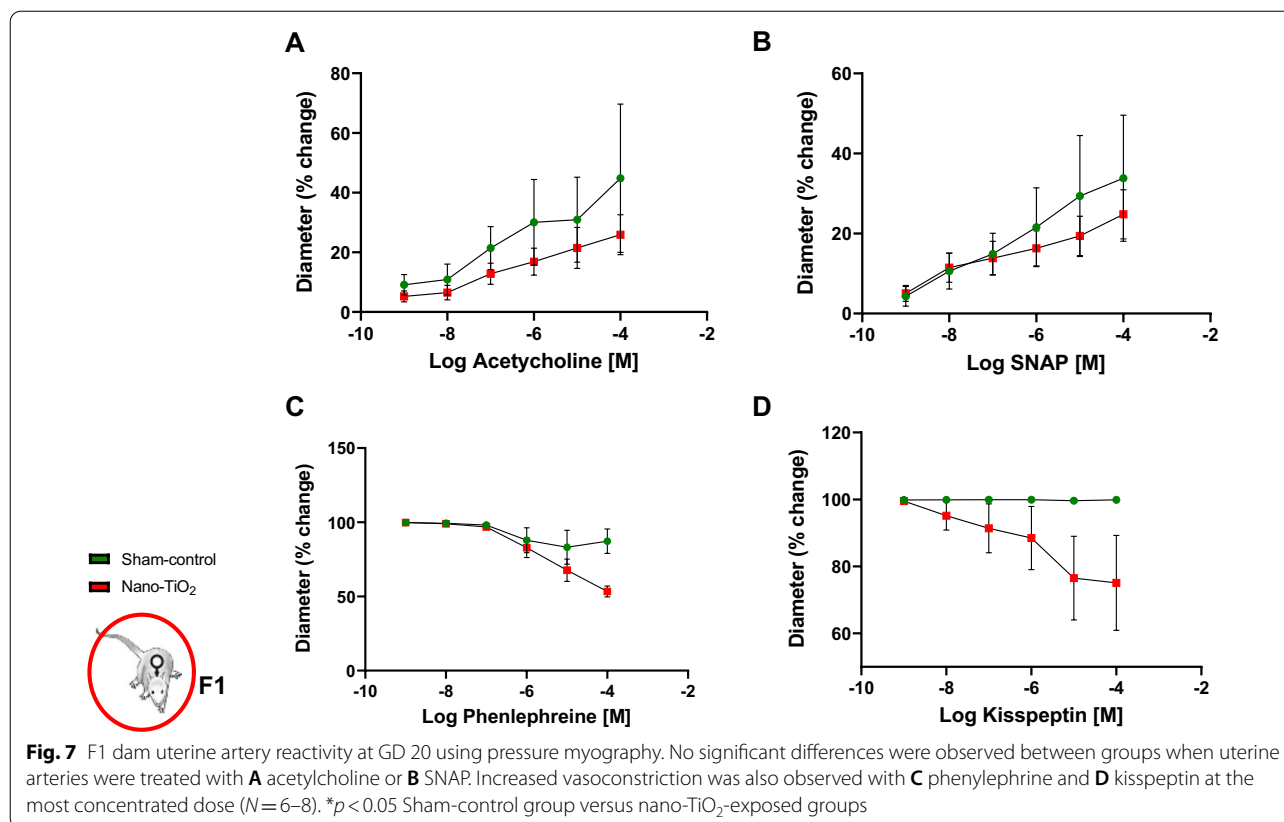
Table 3 Uterine artery characteristics in F1 dams



	n	Inner diameter (μ m)	Wall thickness (μ m)	Tone (%)	Passive diameter outer (μ m)	Passive wall thickness (μ m)
Sham-control	6	591 ± 35	58 ± 7	25 ± 2	705 ± 40	46 ± 4
Nano-TiO₂ exposed	8	$502 \pm 29^*$	50 ± 5	$38 \pm 4^*$	643 ± 27	47 ± 5

Uterine artery characteristics in sham-control (N=6) and nano-TiO₂ inhalation exposed (N=8) groups. Values are shown as mean \pm SEM.

* $p < 0.05$ Sham-control group versus nano-TiO₂-exposed groups.



or independent dilators (Fig. 7A, B). Mechanistically, we were interested if Kiss directly elicited myosin light chain (MLC) phosphorylation. We found that Kiss treatment of aortic smooth muscle cells resulted in a rapid phosphorylation of MLC (Fig. 8A). In addition, we assessed H₂O₂ production capacity in isolated uterine arteries at GD 20 and found elevated H₂O₂ capacity in F1 TiO₂ females (Fig. 8B), which was similar to findings in the aorta of their aged matched male litter mates. These data demonstrate that vascular and redox dysfunction, specifically an increased vasoconstrictor response potentially mediated by increased MLC phosphorylation and elevated uterine artery H₂O₂ capacity, during gestation generationally persists in the F1 dams born to nano-TiO₂ mothers.

Assessment of plasma hormones at gestational day 20 in F1 dams

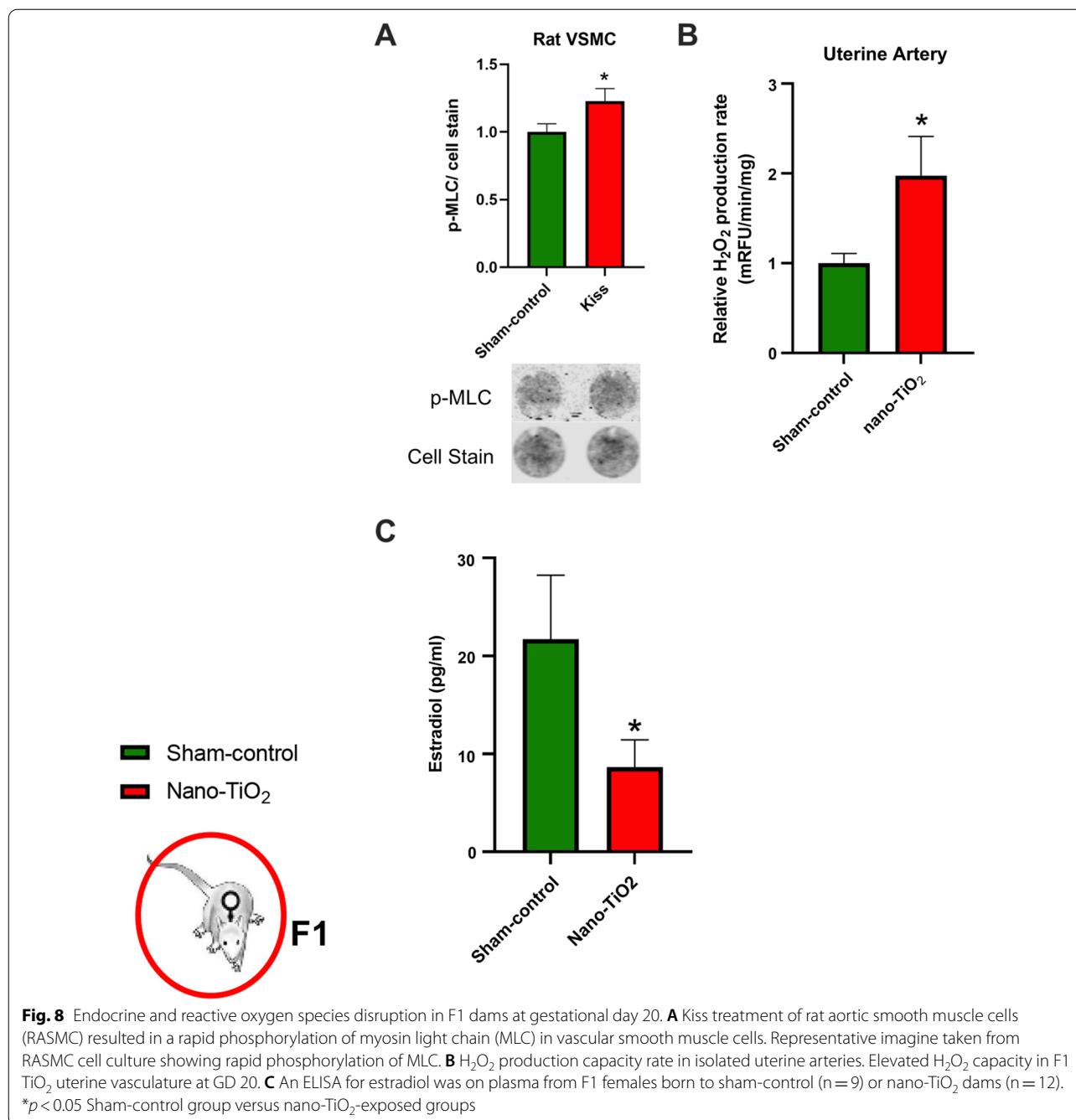
Circulating estrogen was significantly decreased at GD 20 in F1 dams with mothers exposed to nano-TiO₂ (12.12 ± 3.1 pg/ml) compared to F1 dams with sham-control mothers (29.81 ± 8.8 pg/ml $p < 0.05$) (Fig. 8C). However, there were no differences in circulating levels of FSH, LH, P4 or Kiss (data not shown). This indicates that endocrine disruption may occur across generations,

and specifically in this case even though these F1 dams were not directly exposed during their gestations.

Discussion

These studies provide critical insight into the mechanisms regulating the multigenerational effects of maternal ENM inhalation exposure. We report that elevated H₂O₂ production capacity potentially corresponds to upregulation of NF- κ B across generations. Furthermore, we provide novel evidence that offspring born to nano-TiO₂ exposed mothers present with systemic endocrine disruption (estrogen) and alterations in circulating biological mediators (IL-6, glucose, protein carbonyls). This is highlighted by plasma exposed hepatic cells increased H₂O₂ production, which is an effect that is mitigated by silencing the p65 subunit of NF- κ B. We also observed uterine artery and fetoplacental unit dysfunction at GD 20 in F1 dams born to mothers exposed to nano-TiO₂ as previously observed in the F0 dams [10]. Taken together these data illustrate hepatic, vascular, and endocrinological dysfunction in the F1 generation due to gestational exposure in their mothers.

Tightly regulated redox signaling is critical in controlling cellular homeostasis. Our data demonstrate that nano-TiO₂ exposure during gestation leads to



systemically upregulated H₂O₂ production capacity and diminished GSH defense. Further, our cell culture experiments suggest not only elevated H₂O₂ production capacity in a non-challenged state but also a greater H₂O₂ production capacity when stimulated by PMA. Considered together, the F1 nano-TiO₂ generation may be ill equipped to handle physiological challenges such as viral infection dietary challenge or disease. Ultimately, elevated or exaggerated oxidant production in the F1

offspring potentially increases their risk of developing cardio-metabolic pathologies [23, 37–41]. Hepatic oxidant production is linked to numerous pathologies including non-alcoholic fatty liver [42, 43], diabetes [44–46], steatosis [47], and cirrhosis [48], which all in turn increase cardiovascular disease risk [49]. Vascular oxidant production is linked to insulin resistance, atherosclerosis, and peripheral artery disease [50]. Whether or not hepatic vascular dysfunction associated with

inhalation exposure during gestation impacts uterine, placental, or fetal vascular health remains to be determined in future studies.

One prominent redox sensitive transcription factor is NF- κ B [26]. Our data reflects an increased NF- κ B activation in maternal liver of dams exposed to nano-TiO₂ as well as liver and aorta of their offspring. The observed elevation of IL-6, glucose, and H₂O₂ could all contribute to activation of NF- κ B [26, 51, 52]. Redox regulation of NF- κ B is complex as both activation and inactivation have been detailed. Redox activation of NF- κ B can occur at many levels: activation of upstream kinases, inactivation of NF- κ B inhibitors, and direct oxidation [53]. Direct oxidation has been reported to decrease the interaction between NF- κ B and DNA in vitro [54]. However, nuclear translocation of oxidized NF- κ B results in interaction with REF-1, reduction, and increased DNA binding [27], a feature shared by other redox activated transcription factors [55]. While the current study defines the relationship between maternal nano-TiO₂ inhalation exposure during gestation, H₂O₂ and NF- κ B, it is very probable that other transcriptional and signaling pathways are also altered. This topic research topic is relatively unexplored and future studies are needed to better understand the redox-mediated regulation of gene expression following inhalation exposure.

NF- κ B over activation may in part account for the great capacity to produce oxidants. Indeed, our cell exposure experiments support the notion that NF- κ B is important in mediating the upregulation of H₂O₂ production capacity induced by F1 nano-TiO₂ plasma. NF- κ B has been shown to regulate a number of oxidant producing enzymes including NADPH oxidases and xanthine oxidase [56–58]. This study shows upregulated NF- κ B and H₂O₂ production capacity in vascular and hepatic tissue. NF- κ B in the vasculature has been linked with increased vasoconstriction [59], remodeling [60], and atherosclerosis [61]. Suggesting offspring of nano-TiO₂ mothers may be at greater risk of these vascular pathologies as they age or experience a secondary insult, such as consuming a western diet. Future studies will be aimed at understanding the mechanisms of this circular relationship between H₂O₂ and NF- κ B by way of understanding oxidant sources, NF- κ B interaction and gene targets in these tissues.

In addition to NF- κ B, exposure to chronically elevated levels of H₂O₂ can lead to alterations in multiple signaling pathways regulating cellular function and gene regulation. Evidence exists suggesting H₂O₂ directly or indirectly, through thiol antioxidant relay, can modify histones regulating chromatin structure and gene expression [62]. Thus, it is possible the observed elevated H₂O₂ production capacity leads to propagation of nano-TiO₂

impact cross generations through alteration in chromatin structure and gene regulation. Future studies can achieve this by utilizing RNA-Seq and Assay for Transposase-Accessible Chromatin with high throughput sequencing (ATAC-Seq) technologies, as well as 3D nuclear imaging techniques.

Having previously shown that the receptor for Kiss, Kiss1R, is present in the uterine vascular smooth muscle layer [10] we examined estrogen and the vasoreactivity of the uterine artery of F1 dams to Kiss to determine if endocrine-mediated vasoconstriction persists across generations. F1 dams born to mothers exposed to nano-TiO₂ had significantly reduced circulating estrogen levels compared to F1 dams born to control mothers at GD 20. This is of particular interest because these rats were not exposed during their gestations but still suffered endocrine disruption. Estrogen has long been known to play a critical role in women's health during gestation specifically regulating uterine and placental blood flow. In specific regards to data presented in this manuscript, estrogen receptor activation is associated with increased antioxidant defense and direct inhibition of NF- κ B activation [63–65]. Additionally, oxidant production has been shown to reduce estrogen production and release. This implies a detrimental feed-forward interaction of oxidant-mediated reduction of estrogen and estrogen deficiency-induced upregulation of oxidant signaling following maternal nano-TiO₂ inhalation exposure.

Uterine arteries from F1 dams born to mothers exposed to nano-TiO₂ had an elevated tone ($38 \pm 4\%$ exposed vs $25 \pm 2\%$ sham-control). This was characterized anatomically by a smaller luminal diameter, increased wall thickness (Table 3), and physiologically by an assumed vasoconstrictor response to Kiss (Fig. 7). These are similar to observations made in the uterine arteries of dams that were directly exposed to nano-TiO₂ [9]. We then tested whether Kiss could induce the phosphorylation of MLC utilizing rat aortic smooth muscle cells. We found that in culture, phosphorylation of MLC increased modestly following 10 min of Kiss exposure. This result suggests a potential mechanism of Kiss induced vasoconstriction in pressurized uterine arteries. Oxidant production and redox signaling have been previously reported to alter vascular tone and remodeling [66]. Thus, we assessed the H₂O₂ production capacity of isolated uterine arteries and found F1 nano-TiO₂ uterine arteries had a greater H₂O₂ production capacity. This is further evidence of redox dysregulation in the F1 generation of mothers exposed to nano-TiO₂. We speculate that redox dysregulation contributes to the increased vasoconstrictive Kiss response as well as the vascular wall thickening.

Collectively, these results suggest decreased blood flow to fetoplacental units in F0 dams exposed to nano-TiO₂

[16] and their F1 offspring during gestation (current data). Indeed, similar to what was previously reported in nano-TiO₂ F1 pups at GD 20, F2 pups measured significantly smaller than air exposed F2 pups. These results indicate that a single period of gestational exposure affects the health of at least two generations and has long-term consequences in male and female adults born to exposed mothers. Propagation of these multigenerational health effects are likely rooted in changes to chromatin structure and gene regulation. Critical insight into mechanisms of nano-TiO₂-induced multigenerational dysfunction could be gained through sequencing and “omic” style approaches.

One limitation of the current study is that the plasma samples for endocrine analysis were only taken a single time point during gestation. Despite estrogen disruption, other key reproductive hormones such as P4, LH, FSH, and Kiss were unchanged at GD 20, which is similar to what we observed in our previous study in samples taken from dams that were directly exposed [10]. Sampling at different key time points such as implantation or placentation could reveal disruption of other gestational and metabolic factors.

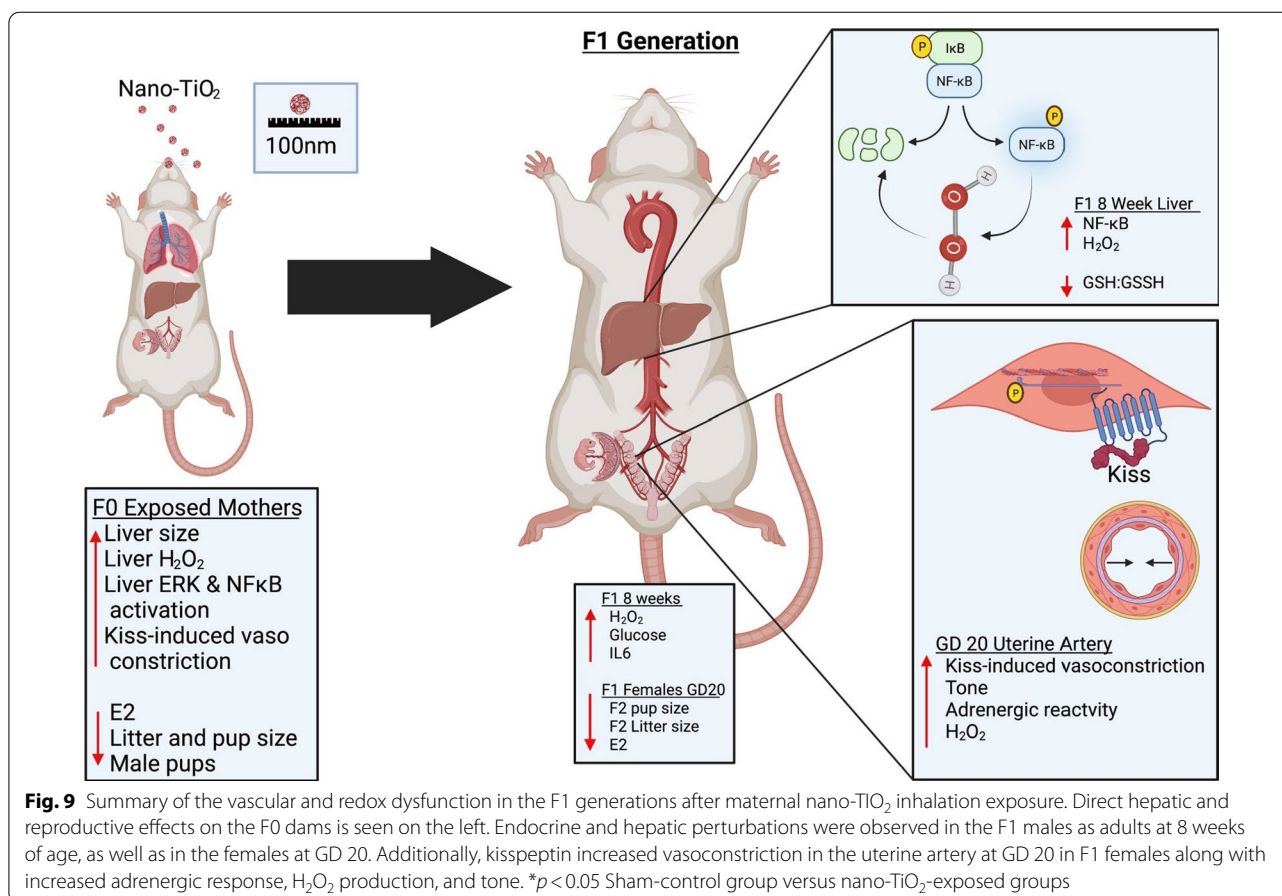
Conclusion

In conclusion, this manuscript provides novel evidence that maternal ENM inhalation exposure results in multi-generational effects. Our data indicate systemic upregulation of H₂O₂ production capacity and NF-κB activation in F0 dams and their offspring (Fig. 9). We speculate that this increases the susceptibility of the F1 generation to various pathologies in adulthood. A focused probe of the F1 uterine vasculature at GD 20 revealed altered gestational function similar to the F0 dams, again resulting in undersized offspring in the F2 generation. The extent of this dysregulation and how long the dysfunction persists and the mechanism by which these outcomes are perpetuated beyond the F1 generation remains a topic ripe for exploration.

Materials and methods

Animal model

Female, Sprague–Dawley (SD rats) were purchased from Hilltop Laboratories (Scottsdale, PA), and housed in an Assessment and Accreditation of Laboratory Animal Care (AAALAC) approved facility at West Virginia University (WVU) under a regulated temperature and



12:12 h light–dark cycle. Rats were randomly assigned to either the sham-control or nano-TiO₂ exposure groups and acclimated for 48–72-h before mating. Rats had ad libitum access to food and water throughout the acclimation period. To increase the likelihood of viable progeny, pregnant rats were exposed to nano-TiO₂ aerosols as described below on or after implantation gestational day 10 (GD 10) as prior indications of inhalation exposure results in near to total loss of pregnancy [15]. Weights of the pregnant dams were recorded weekly. Dams were allowed to deliver pups naturally. Pups were housed with dams for 21 days and weaned based on sex. Once female pups (F1 females) reached sexual maturity (6–8 weeks of age) they were mated to control males to establish pregnancy and euthanized on GD 20. All procedures were approved by the Institutional Animal Care and Use Committee of West Virginia University.

Engineered nanomaterial

Nano-TiO₂ powder was obtained from Evonik (Aeroxide TiO₂, Parsippany, NJ). It is a mixture composed of anatase (80%) and rutile (20%) TiO₂. Particle characteristics have been determined including the primary particle size (21 nm), the specific surface area (48.08 m²/g), and the Zeta potential (−56.6 mV) [7].

Aerosol size distributions were determined in the exposure chamber while the target mass concentration was being maintained at 12 ± 0.13 mg/m³ with: (1) a high-resolution electrical low-pressure impactor (ELPI+; Dekati, Tampere, Finland), (2) a scanning particle mobility sizer (SMPS 3938; TSI Inc., St. Paul, MN), and (3) an aerodynamic particle sizer (APS 3321; TSI Inc., St. Paul, MN), and a Nano Micro-Orifice Uniform Deposit Impactor (MOUDI 115R, MSP Corp, Shoreview, MN).

Inhalation exposure

Nano-TiO₂ aerosols were generated using a high-pressure acoustical generator (HPAG, IESTechno, Morgantown, WV). The output of the generator was fed into a Venturi pump (JS-60 M, Vaccon, Medway, MA) which further de-agglomerated the particles. The nano-TiO₂ aerosol/air mix then entered the whole-body exposure chamber. A personal DataRAM (pDR-1500; Thermo Environmental Instruments Inc., Franklin, MA) was utilized to sample the exposure chamber air to determine the aerosol mass concentration in real-time. Feedback loops within the software automatically adjusted the acoustic energy to maintain a stable mass concentration during the exposure. Gravimetric measurements were conducted on Teflon filters concurrently with the DataRAM measurements to obtain a calibration factor. The gravimetric measurements were also conducted during each exposure to calculate the mass concentration measurements

reported in the study. Bedding material soaked with water was used in the exposure chamber to maintain humidity (30–70%) during exposures. Sham-control animals were exposed to HEPA filtered air only with similar temperature and humidity chamber conditions.

Inhalation exposures in F0 dams lasted for 6 days after GD 10 to decrease animal stress. The pregnant rats were exposed to an average target concentration of 12 mg/m³. This concentration was chosen to match our previous late gestation inhalation exposure studies [14, 15] To estimate lung dose with nano-TiO₂ aerosols [13] we used the equation: $D = F \cdot V \cdot C \cdot T$, where F is the deposition fraction (10%), V is the minute ventilation (208.3 cc), C equals the mass concentration (mg/m³), and T equals the exposure duration (minutes) [67]. This exposure paradigm (12 mg/m³, 6 h/exposure, 6 days) produced an estimated target lung dose of 525 ± 16 µg with the last exposure conducted 24 h prior to sacrifice and experimentation. These calculations represent total lung deposition and do not account for clearance (MPPD Software v 2.11, Arlington, VA).

Enzyme linked immunosorbent assay (ELISA)

F1 Dams were anesthetized with isoflurane gas (5% induction, 2–3.5% maintenance). The animals were placed on a heating pad to maintain a 37 °C rectal temperature. The trachea was intubated to ensure an open airway and the right carotid artery was cannulated to allow for blood sampling of ~3 mL. Plasma and serum were collected on GD 20 and ELISAs were performed for estrogen, progesterone (P4), luteinizing hormone (LH), and follicle stimulating hormone (FSH). All kits were performed according to the recommendation of the manufacturer (CalBiotech, Spring Valley, CA). Additionally, plasma was collected at 8 weeks of age in F1 males and females was assayed for IL-6 (R&D Systems, Minneapolis, MN), glucose (Cayman, Ann Arbor, MI), and plasma protein carbonyls (Abcam, Cambridge, MA). Enzymatic activity for ALT and AST were measured with plasma from F0 dams at GD 20 (n = 8) and F1 at 8 weeks of age (n = 8) samples following the manufacturer's instructions (Cayman, Ann Arbor, MI).

Gestational outcomes in F0 and F1 dams

Litter size, sex ratio, implantation sites, and uterine weights were recorded in F0 and F1 dams. Once trunk blood was collected from F1 dams, F2 pups and placenta were carefully dissected away from the uterine wall and weighed individually immediately after sacrifice (wet weight) and after desiccation (dry weight). F2 pup and placental weights were measured to calculate placental efficiency (grams fetus/gram placental).

Cell culture

AML12 hepatocytes were grown in DMEM/F12 (ThermoFisher Scientific, Waltham, MA) media supplemented with dexamethasone, (ThermoFisher Scientific, Waltham, MA) growth supplement (ThermoFisher Scientific, Waltham, MA), and 10% FBS (ThermoFisher Scientific, Waltham, MA). For plasma exposure AML12 cells were seeded in a clear bottom black sided 96-well plate (ThermoFisher Scientific, Waltham, MA) and allowed to adhere for 24 h. At ~90% confluency the media was replaced with plasma samples mixed with 2 parts culture media and incubated for 1 h prior to H₂O₂ measurements. In other experiments AML12 cells were reverse transfected using lipofectamine 3000 with 10 nM of either scrambled or p65 targeted siRNA (ThermoFisher Scientific, Waltham, MA) when plated in the 96-well plates. Cells were grown in these conditions for 48 h. Then media was replaced with plasma (collected from F1 offspring at 8 weeks of age; n = 8) spiked culture media as above and left overnight before assessing H₂O₂ measurements.

Rat Aortic smooth muscle cells (RASMC) were grown in Lonza smooth muscle complete media (Lonza, Basel, Switzerland). For experiments RASMC were plated in 6-well or clear bottom black sided 96-well plate. Cells were then exposed to 1 ng/ml of Kiss for the times indicated (0, 5, or 10 min) and 96-well plates fixed for in-cell western.

Coumarin boronic acid assay

Coumarin Boronic acid (CBA) was conducted as previously published [55, 68–71]. Tissue was homogenized in PBS (Fisher Scientific, Waltham, MA) containing a protease and phosphatase cocktail (ThermoFisher Scientific, Waltham, MA). 10 µl of equal concentration sample homogenate were loaded into a black sided 96 well plate along with 90 µl of CBA buffer (containing PBS, L-Name (Sigma-Aldrich, St. Louis, MO), Taurine (Sigma-Aldrich, St. Louis, MO), and 500 µM CBA probe (Cayman, Ann Arbor, MI) ± 1 KU catalase (Sigma-Aldrich, St. Louis, MO). For 96-well plates cell culture media was removed and 100 µl of CBA buffer (again containing 500 µM of CBA probe) was added ± 1 KU catalase. Plates were then run in a 37 °C plate reader and fluorescence measured (ex: 350, em: 450) every minute over 2 h. Signal from the negative control catalase wells were subtracted out from the sample wells and only the catalase inhibitable signal was analyzed. The rate of the relative fluorescent units per minute was calculated for all samples and fold change from control treatment calculated.

Glutathione assay

Samples were prepared and according to the kit protocol (ab239709, Abcam, Cambridge, MA). In brief, aorta and liver were homogenized in assay buffer and each sample was run with and without glutathione reductase to measure total GSH, reduced GSH, and calculate the oxidized to reduced ratio.

Western blot

Medial lobe liver sections were snap frozen at the time of euthanasia. Liver tissue was homogenized in RIPA buffer containing a protease and phosphatase cocktail (ThermoFisher, Waltham, MA). Samples were then prepared with laemmli sample buffer and β-mercaptoethanol at a 4 µg/µl concentration and 32 µg of total protein run down each lane of a 4–20% gradient gel (Biorad, Hercules, California) at 70 V. Samples were then transferred to 0.45 µm nitrocellulose membranes, dried, reconstituted with ddH₂O, blocked with LiCor (Lincoln, Nebraska) TBS blocking buffer, and incubated in primary antibody overnight at 4 °C. Primary antibodies include β-actin (Santa Cruz Biotechnology, Dallas, Texas), phospho myosin light chain (Thr18/Ser19) (Cell Signaling Technologies, Danvers, MA), phospho and total p65 (Cell Signaling Technologies, Danvers, MA), phospho and total ERK 1/2 (Cell Signaling Technologies, Danvers, MA), and catalase (Abcam, Cambridge MA). Membranes were then washed with TBS containing 1% tween (TBST), incubated in Licor near-infrared secondary antibodies for 1 h at room temperature, washed again with TBST, and finally imaged with the LiCor Odyssey Clx. Densitometry analysis was conducted in Image-J (National Institutes of Health, Bethesda, Maryland) with phosphor-signal normalized to total-signal and fold change calculated from control.

Isolated microvessel protocol (pressure myography)

After the placenta and pups were removed, uteri were placed in a dissecting dish with physiological salt solution (PSS), as previously described [72], and maintained at 4 °C. A uterine artery segment was isolated, removed and transferred to a vessel chamber (Living Systems Instrumentation, Burlington, VT) containing fresh oxygenated PSS, cannulated with glass pipettes, and secured using nylon suture (11-0 ophthalmic, Alcon, U.K.). Arteries were extended to their in-situ length, pressurized to 60 mm Hg with PSS, superfused with warmed.

(37 °C) oxygenated PSS at a rate of 10 mL/min, and allowed to develop spontaneous tone. Internal and external arteriolar diameters were measured using video calipers (Colorado Video, Boulder, CO).

Uterine vasculature reactivity

Uterine arteries were allowed to develop spontaneous tone, defined as the degree of constriction experienced by a blood vessel relative to its maximally dilated state. Vascular tone ranges from 0% (maximally dilated) to 100% (maximal constriction). Vessels with a spontaneous tone $\geq 20\%$ less than initial tone were included in this study. After equilibration, parameters of arterial vasoreactivity were analyzed. Vessels that did not develop sufficient spontaneous tone were not included in the data analysis.

Assessment of vasoreactivity

Arteries were exposed to increasing concentrations of phenylephrine (PE: 10^{-9} to 10^{-4} M), acetylcholine (ACh: 10^{-9} to 10^{-4} M), sodium nitroprusside (SNP: 10^{-9} to 10^{-4} M) and kisspeptin-10 (Kiss: 10^{-9} to 10^{-4} M), which were each added separately to the bath. The steady state diameter of the vessel was recorded for at least 2 min after each dose. After each dose curve was completed, the vessel bath was exchanged to remove excess chemicals by carefully removing the superfusate and replacing it with fresh warmed oxygenated PSS. After all experimental treatments were complete, the PSS was replaced with Ca^{2+} -free PSS until maximum passive diameter was established.

Pressure myography calculations

Spontaneous tone was calculated by the following equation:

$$\text{Spontaneous tone}(\%) = \left\{ \frac{(D_m - D_i)}{D_i} \right\} \times 100$$

where D_m is the maximal diameter and D_i is the initial steady state diameter recorded prior to the experiment. Active responses to pressure were normalized to the maximal diameter using the following formula:

$$\text{Normalized diameter} = D_{ss}/D_m$$

where D_{ss} is the steady state diameter recorded during each pressure change. The experimental responses to ACh, PE, and SNP are expressed using the following equation:

$$\text{Diameter}(\text{percent maximal diameter}) = \left\{ \frac{(D_{ss} - D_{con})}{(D_m - D_{con})} \right\} \times 100$$

where D_{con} is the control diameter recorded prior to the dose curve, D_{ss} is the steady state diameter at each dose of the curve. The experimental response to PE is expressed using the following equation:

$$\text{Diameter}(\text{percent maximal diameter}) = \left\{ \frac{(D_{con} - D_{ss})}{(D_{con})} \right\} \times 100$$

Wall thickness (WT) was calculated from the measurement of both inner (ID) and outer (OD) steady state arteriolar diameters at the end of the Ca^{2+} free wash using the following equation:

$$WT = (OD - ID)/2.$$

Statistics

Data are expressed as means \pm standard error of the mean. Point-to-point differences in the dose response curves were evaluated using two-way repeated measures analysis of variance (ANOVA) with a Tukey's *post-hoc* analysis when significance was found. The animal characteristics, vessel characteristics and hepatocytes transfected with siRNA were analyzed using a one-way ANOVA with a Tukey *post-hoc* analysis when significance was found. Student's t-test was utilized for comparison of two groups (i.e. liver weights). All statistical analysis was completed with Graph Pad Prism (San Diego, CA) Significance was set at $p < 0.05$, N is the number of animals per group, n is the number of vessels per group.

Supplementary Information

The online version contains supplementary material available at <https://doi.org/10.1186/s12989-022-00457-y>.

Additional file 1. Figure S1: Hydrogen peroxide production rate in additional tissues from F1 males at 8 weeks of age. H_2O_2 production capacity detected by coumarin boronic acid in other F1 tissue A) pancreas, B) lung, C) brain. $n=4-20$. *, $p < 0.05$ Sham-control group versus nano-TiO₂-exposed groups. Hepatocytes transfected with scrambled or p65 targeted siRNA were exposed overnight to 1:2 diluted F1 plasma then phosphorylation status determined ($n=6$); *, $p < 0.05$ Sham-control group versus nano-TiO₂-exposed groups.

Additional file 2. Table S1: Pup and Placental Characteristics from F1 Dams. Pup and placental characteristics in sham-control ($N = 9$) and nano-TiO₂ inhalation exposed ($N = 10$) groups. Values are shown as mean \pm SEM. $P \leq 0.05$, * Sham control group vs. nano-TiO₂ exposed groups.

Acknowledgements

The authors would like to thank the West Virginia University Imaging Facilities where imaging experiments and image analysis were performed and have been supported by the WVU Cancer Institute and NIH grants P20RR016440 and P30RR032138/P30GM103488.

Authors' contributions

Study design: EB/ED/TN. Data collection: EB/ED/JG/KG/KW/KE/TB/WG/KS/MS. Data analysis and interpretation: EB/ED/SH/TN. Manuscript draft: EB/ED. Critical revision and final decision to submit: all authors. The author(s) read and approved the final manuscript.

Funding

This work was supported by the following sources: National Institutes of Health R01 ES015022 (TRN) and WV-CTSI U54 GM104942-05 (ECB), NHLBI F32 HL152534-01 (ERD), R01 ES031253 (SH).

Declarations

Ethics approval and consent to participate

Animal studies were reviewed and approved by the Animals Care and Use Committee at West Virginia University (#160200621).

Consent for publication

Not applicable.

Competing interests

Authors declare that they have no competing interests.

Author details

¹Department of Physiology and Pharmacology, 64 Medical Center Drive, Robert C. Byrd Health Sciences Center, West Virginia University School of Medicine, West Virginia University, Morgantown, WV 26505-9229, USA. ²Center for Inhalation Toxicology, West Virginia University School of Medicine, Morgantown, WV, USA.

Received: 23 September 2021 Accepted: 24 February 2022

Published online: 09 March 2022

References

- Bustamante JJ, Copple BL, Soares MJ, Dai G. Gene profiling of maternal hepatic adaptations to pregnancy. *Liver Int.* 2010;30:406–15.
- Zeng Z, Liu F, Li S. Metabolic adaptations in pregnancy: a review. *Ann Nutr Metab.* 2017;70:59–65.
- Sanghavi M, Rutherford JD. Cardiovascular physiology of pregnancy. *Circulation.* 2014;130:1003–8.
- Birnbaum LS. State of the science of endocrine disruptors. *Environ Health Persp.* 2013;121:a107–a107.
- Gillman MW, Barker D, Bier D, Cagampang F, Challis J, Fall C, et al. Meeting report on the 3rd international congress on developmental origins of health and disease (DOHaD). *Pediatr Res.* 2007;61:625–9.
- Barker DJP. The origins of the developmental origins theory. *J Intern Med.* 2007;261:412–7.
- Knudsen TM, Rezwan FI, Jiang Y, Karmaus W, Svanes C, Holloway JW. Transgenerational and intergenerational epigenetic inheritance in allergic diseases. *J Allergy Clin Immunol.* 2018;142:765–72.
- D'Errico JN, Fournier SB, Stapleton PA. Ex vivo perfusion of the rodent placenta. *J Vis Exp.* 2019.
- Fournier SB, D'Errico JN, Adler DS, Kollontzi S, Goedken MJ, Fabris L, et al. Nanopolystyrene translocation and fetal deposition after acute lung exposure during late-stage pregnancy. *Part Fibre Toxicol.* 2020;17:55.
- Bowdridge EC, Abukabda AB, Engles KJ, McBride CR, Batchelor TP, Goldsmith WT, et al. Maternal engineered nanomaterial inhalation during gestation disrupts vascular kisspeptin reactivity. *Toxicol Sci.* 2019;169:524–33.
- Hansen SF, Larsen BH, Olsen SI, Baun A. Categorization framework to aid hazard identification of nanomaterials. *Nanotoxicology.* 2009;1:243–50.
- Ellenbecker MJ, Tsai CS. Exposure assessment and safety considerations for working with engineered nanoparticles. 2015;269–84.
- Nurkiewicz TR, Porter DW, Hubbs AF, Cumpston JL, Chen BT, Frazer DG, et al. Nanoparticle inhalation augments particle-dependent systemic microvascular dysfunction. *Part Fibre Toxicol.* 2008;5:1.
- Stapleton PA, McBride CR, Yi J, Abukabda AB, Nurkiewicz TR. Estrous cycle-dependent modulation of in vivo microvascular dysfunction after nanomaterial inhalation. *Reprod Toxicol.* 2018;78:20–8.
- Stapleton PA, Minarchick VC, Yi J, Engels K, McBride CR, Nurkiewicz TR. Maternal engineered nanomaterial exposure and fetal microvascular function: does the Barker hypothesis apply? *Am J Obstet Gynecol.* 2013;209:227.e1–227.e11.
- Abukabda AB, Bowdridge EC, McBride CR, Batchelor TP, Goldsmith WT, Garner KL, et al. Maternal titanium dioxide nanomaterial inhalation exposure compromises placental hemodynamics. *Toxicol Appl Pharm.* 2019;367:51–61.
- Kotani M, Dethoux M, Vandenbogaerde A, Communi D, Vanderwinden J-M, Poul EL, et al. The metastasis suppressor gene KISS-1 encodes kisspeptins, the natural ligands of the orphan G protein-coupled receptor GPR54*. *J Biol Chem.* 2001;276:34631–6.
- Bilban M, Ghaffari-Tabrizi N, Hintermann E, Bauer S, Molzer S, Zoratti C, et al. Kisspeptin-10, a KISS-1/metastatin-derived decapeptide, is a physiological invasion inhibitor of primary human trophoblasts. *J Cell Sci.* 2004;117:1319–28.
- de Roux N, Genin E, Carel J-C, Matsuda F, Chaussain J-L, Milgrom E. Hypogonadotropic hypogonadism due to loss of function of the KISS1-derived peptide receptor GPR54. *Proc Natl Acad Sci.* 2003;100:10972–6.
- Cetković A, Miljic D, Ljubić A, Patterson M, Ghatei M, Stamenković J, et al. Plasma Kisspeptin levels in pregnancies with diabetes and hypertensive disease as a potential marker of placental dysfunction and adverse perinatal outcome. *Endocr Res.* 2012;37:78–88.
- Tassigny X, Colledge WH. The role of Kisspeptin signaling in reproduction. *Physiology.* 2010;25:207–17.
- Perez-Torres I, Guarner-Lans V, Rubio-Ruiz ME. Reductive stress in inflammation-associated diseases and the pro-oxidant effect of antioxidant agents. *Int J Mol Sci.* 2017;18:2098.
- DeVallance E, Li Y, Jurczak MJ, Cifuentes-Pagano E, Pagano PJ. The role of NADPH oxidases in the etiology of obesity and metabolic syndrome: contribution of individual isoforms and cell biology. *Antioxid Redox Sign.* 2019;31:687–709.
- Foyer CH, Noctor G. Redox homeostasis and antioxidant signaling: a metabolic interface between stress perception and physiological responses. *Plant Cell Online.* 2005;17:1866–75.
- He L, He T, Farrar S, Ji L, Liu T, Ma X. Antioxidants maintain cellular redox homeostasis by elimination of reactive oxygen species. *Cell Physiol Biochem.* 2017;44:532–53.
- Takada Y, Mukhopadhyay A, Kundu GC, Mahabeshwar GH, Singh S, Aggarwal BB. Hydrogen peroxide activates NF-kappa B through tyrosine phosphorylation of I kappa B alpha and serine phosphorylation of p65: evidence for the involvement of I kappa B alpha kinase and Syk protein-tyrosine kinase. *J Biol Chem.* 2003;278:24233–41.
- Kabe Y, Ando K, Hirao S, Yoshida M, Handa H. Redox regulation of NF-kappaB activation: distinct redox regulation between the cytoplasm and the nucleus. *Antioxid Redox Sign.* 2005;7:395–403.
- Fiordelisi A, Iaccarino G, Morisco C, Coscioni E, Sorriento D. NFkappaB is a key player in the crosstalk between inflammation and cardiovascular diseases. *Int J Mol Sci.* 2019;20:1599.
- Papa S, Bubici C, Zazzeroni F, Franzoso G. Mechanisms of liver disease: cross-talk between the NF-kappaB and JNK pathways. *Biol Chem.* 2009;390:965–76.
- Leikauf GD, Kim S-H, Jang A-S. Mechanisms of ultrafine particle-induced respiratory health effects. *Exp Mol Medicine.* 2020;52:329–37.
- Madl AK, Plummer LE, Carosino C, Pinkerton KE. Nanoparticles, lung injury, and the role of oxidant stress. *Annu Rev Physiol.* 2014;76:447–65.
- Li N, Xia T, Nel AE. The role of oxidative stress in ambient particulate matter-induced lung diseases and its implications in the toxicity of engineered nanoparticles. *Free Radical Bio Med.* 2008;44:1689–99.
- Rao X, Zhong J, Brook RD, Rajagopalan S. Effect of particulate matter air pollution on cardiovascular oxidative stress pathways. *Antioxid Redox Sign.* 2018;28:797–818.
- Araujo JA. Particulate air pollution, systemic oxidative stress, inflammation, and atherosclerosis. *Air Qual Atmosphere Heal.* 2010;4:79–93.
- Veal EA, Day AM, Morgan BA. Hydrogen peroxide sensing and signaling. *Mol Cell.* 2007;26:1–14.
- Basini G, Grasselli F, Bussolati S, Ciccimarra R, Maranesi M, Bufalari A, et al. Presence and function of kisspeptin/KISS1R system in swine ovarian follicles. *Theriogenology.* 2018;115:1–8.
- Foyer CH, Noctor G. Redox homeostasis and antioxidant signaling: a metabolic interface between stress perception and physiological responses. *Plant Cell.* 2005;17:1866–75.
- Witting PK, Rayner BS, Wu B-J, Ellis NA, Stocker R. Hydrogen peroxide promotes endothelial dysfunction by stimulating multiple sources of superoxide anion radical production and decreasing nitric oxide bioavailability. *Cell Physiol Biochem.* 2007;20:255–68.
- Cai H. Hydrogen peroxide regulation of endothelial function: origins, mechanisms, and consequences. *Cardiovasc Res.* 2005;68:26–36.
- Stocker R, Kearney JF. Role of oxidative modifications in atherosclerosis. *Physiol Rev.* 2004;84:1381–478.

41. Park J-G, Yoo J-Y, Jeong S-J, Choi J-H, Lee M-R, Lee M-N, et al. Peroxiredoxin 2 deficiency exacerbates atherosclerosis in apolipoprotein E-deficient mice. *Circ Res*. 2011;109:739–49.
42. Mehta K, Thiel DH, Shah N, Mobarhan S. Nonalcoholic fatty liver disease: pathogenesis and the role of antioxidants. *Nutr Rev*. 2002;60:289–93.
43. Matsumoto M, Zhang J, Zhang X, Liu J, Jiang JX, Yamaguchi K, et al. The NOX1 isoform of NADPH oxidase is involved in dysfunction of liver sinusoids in nonalcoholic fatty liver disease. *Free Radical Bio Med*. 2018;115:412–20.
44. Fang H, Feng Q, Shi Y, Zhou J, Wang Q, Zhong L. Hepatic insulin resistance induced by mitochondrial oxidative stress can be ameliorated by sphingosine 1-phosphate. *Mol Cell Endocrinol*. 2020;501:110660.
45. Patche J, Girard D, Catan A, Boyer F, Dobi A, Planesse C, et al. Diabetes-induced hepatic oxidative stress: a new pathogenic role for glycated albumin. *Free Radical Bio Med*. 2017;102:133–48.
46. Kumashiro N, Tamura Y, Uchida T, Ogihara T, Fujitani Y, Hirose T, et al. Impact of oxidative stress and peroxisome proliferator-activated receptor gamma coactivator-1alpha in hepatic insulin resistance. *Diabetes*. 2008;57:2083–91.
47. Prieto I, Monsalve M. ROS homeostasis, a key determinant in liver ischemic-preconditioning. *Redox Biol*. 2017;12:1020–5.
48. Stirpe F, Ravaoli M, Battelli MG, Musiani S, Grazi GL. Xanthine oxidoreductase activity in human liver disease. *Am J Gastroenterol*. 2002;97:2079–85.
49. Tana C, Ballestri S, Ricci F, Vincenzo AD, Ticinesi A, Gallina S, et al. Cardiovascular risk in non-alcoholic fatty liver disease: mechanisms and therapeutic implications. *Int J Environ Res Pu*. 2019;16:3104.
50. Madamanchi NR, Vendrov A, Runge MS. Oxidative stress and vascular disease. *Arterioscler Thromb Vasc Biol*. 2005;25:29–38.
51. Brasier AR. The nuclear factor-kappaB-interleukin-6 signalling pathway mediating vascular inflammation. *Cardiovasc Res*. 2010;86:211–8.
52. Romeo G, Liu WH, Asnaghi V, Kern TS, Lorenzi M. Activation of nuclear factor-kappaB induced by diabetes and high glucose regulates a proapoptotic program in retinal pericytes. *Diabetes*. 2002;51:2241–8.
53. Lingappan K. NF-kappaB in oxidative stress. *Curr Opin Toxicol*. 2018;7:81–6.
54. Gambhir L, Checker R, Sharma D, Thoh M, Patil A, Degani M, et al. Thiol dependent NF-kappaB suppression and inhibition of T-cell mediated adaptive immune responses by a naturally occurring steroidal lactone Withaferin A. *Toxicol Appl Pharm*. 2015;289:297–312.
55. Jesus DS, DeVallance E, Li Y, Falabella M, Guimaraes D, Shiva S, et al. Nox1/Ref-1-mediated activation of CREB promotes Gremlin1-driven endothelial cell proliferation and migration. *Redox Biol*. 2019;22:101138.
56. Martinez-Hervas S, Real JT, Ivorra C, Priego A, Chaves FJ, Pallardo FV, et al. Increased plasma xanthine oxidase activity is related to nuclear factor kappa beta activation and inflammatory markers in familial combined hyperlipidemia. *Nutr Metab Cardiovasc Dis*. 2010;20:734–9.
57. Anrather J, Racchumi G, Iadecola C. NF-kappaB regulates phagocytic NADPH oxidase by inducing the expression of gp91phox. *J Biol Chem*. 2006;281:5657–67.
58. Morgan MJ, Liu ZG. Crosstalk of reactive oxygen species and NF-kappaB signaling. *Cell Res*. 2011;21:103–15.
59. Xie H, Ray PE, Short BL. NF-kappaB activation plays a role in superoxide-mediated cerebral endothelial dysfunction after hypoxia/reoxygenation. *Stroke*. 2005;36:1047–52.
60. Saito T, Hasegawa Y, Ishigaki Y, Yamada T, Gao J, Imai J, et al. Importance of endothelial NF-kappaB signalling in vascular remodelling and aortic aneurysm formation. *Cardiovasc Res*. 2013;97:106–14.
61. de Winther MP, Kanters E, Kraal G, Hofker MH. Nuclear factor kappaB signaling in atherogenesis. *Arterioscler Thromb Vasc Biol*. 2005;25:904–14.
62. Kreuz S, Fischle W. Oxidative stress signaling to chromatin in health and disease. *Epigenomics-uk*. 2016;8:843–62.
63. Xing D, Oparil S, Yu H, Gong K, Feng W, Black J, et al. Estrogen modulates NFkappaB signaling by enhancing IkappaBalpha levels and blocking p65 binding at the promoters of inflammatory genes via estrogen receptor-beta. *PLoS ONE*. 2012;7:e36890.
64. Lean JM, Jagger CJ, Kirstein B, Fuller K, Chambers TJ. Hydrogen peroxide is essential for estrogen-deficiency bone loss and osteoclast formation. *Endocrinology*. 2005;146:728–35.
65. Murphy AJ, Guyre PM, Pioli PA. Estradiol suppresses NF-kappa B activation through coordinated regulation of let-7a and miR-125b in primary human macrophages. *J Immunol*. 2010;184:5029–37.
66. Nedeljkovic ZS, Gokce N, Loscalzo J. Mechanisms of oxidative stress and vascular dysfunction. *Postgrad Med J*. 2003;79:195.
67. Yi J, Chen BT, Schwegler-Berry D, Frazer D, Castranova V, McBride C, et al. Whole-body nanoparticle aerosol inhalation exposures. *J Vis Exp*. 2013;2013:e50263.
68. DeVallance E, Branyan KW, Lemaster KC, Anderson R, Marshall KL, Olfert IM, et al. Exercise training prevents the perivascular adipose tissue-induced aortic dysfunction with metabolic syndrome. *Redox Biol*. 2019;26:101285.
69. Li Y, Cifuentes-Pagano E, DeVallance ER, de Jesus DS, Sahoo S, Meijles DN, et al. NADPH oxidase 2 inhibitors CPP11G and CPP11H attenuate endothelial cell inflammation & vessel dysfunction and restore mouse hind-limb flow. *Redox Biol*. 2019;22:101143.
70. Novelli EM, Little-Ihrig L, Knupp HE, Rogers NM, Yao M, Baust JJ, et al. Vascular TSP1-CD47 signaling promotes sickle cell-associated arterial vasculopathy and pulmonary hypertension in mice. *Am J Physiol-Lung C*. 2019;316:L1150–64.
71. DeVallance ER, Branyan KW, Olfert IM, Pistilli EE, Bryner RW, Kelley EE, et al. Chronic stress induced perivascular adipose tissue impairment of aortic function and the therapeutic effect of exercise. *Exp Physiol*. 2021;106:1343–58.
72. Nurkiewicz TR, Porter DW, Barger M, Castranova V, Boegehold MA. Particulate matter exposure impairs systemic microvascular endothelium-dependent dilation. *Environ Health Persp*. 2004;112:1299–306.

Publisher's Note

Springer Nature remains neutral with regard to jurisdictional claims in published maps and institutional affiliations.

Ready to submit your research? Choose BMC and benefit from:

- fast, convenient online submission
- thorough peer review by experienced researchers in your field
- rapid publication on acceptance
- support for research data, including large and complex data types
- gold Open Access which fosters wider collaboration and increased citations
- maximum visibility for your research: over 100M website views per year

At BMC, research is always in progress.

Learn more biomedcentral.com/submissions

